Existence of a liquid-liquid phase transition in methanol

Matej Huš and Tomaz Urbic*

Chair of Physical Chemistry, Faculty of Chemistry and Chemical Technology, University of Ljubljana, Večna pot 113, SI-1000 Ljubljana, Slovenia

(Received 26 February 2014; revised manuscript received 13 September 2014; published 5 December 2014)

A simple model is constructed to study the phase diagram and thermodynamic properties of methanol, which is described as a dimer of an apolar sphere mimicking the methyl group and a sphere with core-softened potential as the hydroxyl group. Performing classical Monte Carlo simulations, we obtained the phase diagram, showing a second critical point between two different liquid phases. Evaluating systems with a different number of particles, we extrapolate to infinite size in accordance with Ising universality class to obtain bulk values for critical temperature, pressure, and density. Strong evidence that the structure of the liquid changes upon transition from high- to low-density phase was provided. From the experimentally determined hydrogen bond strength and length in methanol and water, we propose where the second critical point of methanol should be.

DOI: 10.1103/PhysRevE.90.062306 PACS number(s): 64.70.Ja, 61.20.Ja

I. INTRODUCTION

Water has been a subject of considerable research effort because of its ubiquity on the surface of the Earth and its importance in life [1,2]. The interest in water is further increased by its peculiar anomalies [3] that distinguish it from many other "common" liquids. The existence of a liquid-liquid (LL) first-order phase transition in supercooled water has been one of the most heavily debated questions [4–6]. The liquid-liquid critical point (LLCP) hypothesis was put forward in 1992 after simulations of the ST2 water model showed a putative phase transition in the supercooled range [7]. Much of the subsequent research was focused on proving or disproving the existence of LLCP and results to this day remain mixed [8–15]. Studies of water in ST2 as well as other models continue to support the LLCP hypothesis, but there is limited experimental evidence to back these claims up because the supposed LLCP is well below the homogenous nucleation temperature of water [16–18]. Phase transition between high-density amorphous (HDA) and low-density amorphous (LDA) ice has often been studied instead [19,20]. Nevertheless, this theory remains credible as it neatly explains the existence of the temperature of maximum density (TMD) in liquid water [7,21,22]. TMD is thought to be a direct consequence of the competition between the translational order at high densities and tetrahedral order (imposed by preferential directions due to strong hydrogen bonding) at low densities, although it is by no means a necessary consequence of the LLCP [23–25].

Mixtures of alcohols and water are equally important, as they find use in food processing and preservation, medical procedures, transportation, and other applications. Methanol is an archetypal example of alcohols. As it is the simplest organic alcohol, it deserves a special attention. It is in many respects similar to water as it, too, forms hydrogen bonds of comparable strength and length (although fewer in number), and its molecule is not much larger than the water molecule. Water and methanol are also fully miscible. There are, however, some important differences, among them the lack of density anomaly, much lower dielectric constant (78.2 for water and 32.7 for methanol), and generally lower melting and boiling points of methanol due to fewer hydrogen bonds [26].

Water is traditionally modeled with explicit models, such as TIP3P [27], SPC/E [28], TIP4P [29], and TIP5P [30]. It has been shown that coarse-grained models, Mercedes-Benz models [31–33], and even soft-core symmetric potentials with two characteristic lengths [34–37] can also reproduce thermodynamics, anomalies, and nonideality remarkably well [38], although there are transferability issues that prevent capturing all thermodynamic properties simultaneously with such models [39]. They are particularly useful to study hydrophobic hydration and effects derived thereof: hydrophobic effect [40], and protein folding [41–43] and denaturation [35,44,45]. Recently, it has been shown that it might be possible to obtain anomalous phase behavior even in soft-core potentials with strictly monotonic force [46] and without two distinct length scales, i.e., under far less stringent conditions than previously thought [47,48].

Here we extend a soft-core water model, originally proposed by Franzese [49], to describe methanol. Computer simulations of methanol have recently become increasingly popular because of the importance of methanol and easier tractability due to modern computing power [50–53]. As Su *et al.* have proved [54], extensions of soft-core potential water models to methanol are physically sound and well founded for they correctly reproduce excess volume and enthalpy for methanol-water mixtures. In this paper, we show that a soft-core model of methanol predicts until now experimentally unobserved LLCP.

This paper is organized as follows. In Sec. II we outline the model details. The method of simulation used is explained in Sec. III. Section IV deals with results and their discussion, which is summed up in the Conclusion.

II. MODEL DETAILS

Methanol is modeled as a pair of tangent spheres (pseudoatoms) of diameter a. They interact with pairwise potentials, shown in Fig. 1. Pseudoatoms representing the hydroxyl

*tomaz.urbic@fkkt.uni-lj.si

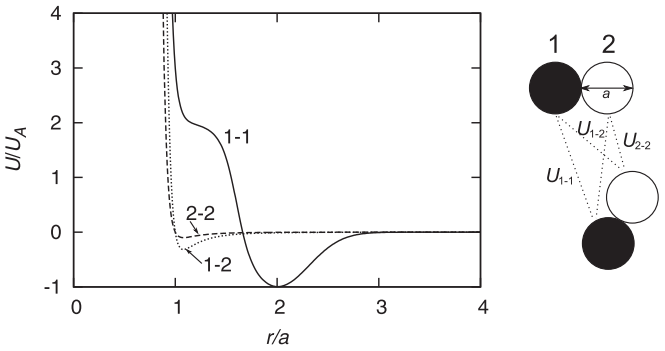

FIG. 1. Methanol is modeled with two pseudoatoms (OH and CH_3) in a fixed position. Interaction between type 1 particles is described by the CSW potential, while other interactions behave like a 24-6 Lennard-Jones potential.

groups (black circles) of methanol interact with the continuous shouldered well (CSW) potential, written as [49]

$$U(r) = \frac{U_R}{1+\exp\left[\Delta\left(r-R_R\right)/a\right]} - U_A \exp\left(-\frac{(r-R_A)^2}{2\delta_A^2}\right) + U_A\left(\frac{a}{r}\right)^{24} \quad (1)$$

and with parameters $U_R/U_A = 2$, $R_R/a = 1.6$, $R_A/a = 2$, $(\delta_A/a)^2 = 0.1$, and $\Delta = 15$ [49]. Interaction between the methyl groups (white circles) and interaction between the methyl and hydroxyl groups are 24-6 Lennard-Jones [34,38,40]

$$U = \frac{4}{3}2^{\frac{2}{3}}\epsilon\left[\left(\frac{\sigma}{r}\right)^{24} - \left(\frac{\sigma}{r}\right)^{6}\right], \quad (2)$$

with parameters $\sigma_{\mathrm{LJ}}/a = 1.0$ and $\epsilon_{\mathrm{LJ}}/U_A = 0.1$, and using Lorentz-Berthelot mixing rules: $\sigma_{\mathrm{mix}} = 0.5\left(\sigma_{\mathrm{LJ}} + a\right)$ and $U_{\mathrm{mix}} = \sqrt{\epsilon_{\mathrm{LJ}} U_A}$ [34,38,40]. For clarity, quantities are reported in reduced dimensionless units relative to the hydroxyl group diameter and the depth of its attractive well: as $T^* = k_B T/U_A$, $\rho^* = \rho a^3$, and $p^* = p a^3/U_A$.

III. SIMULATION DETAILS

To construct a phase diagram, several Monte Carlo simulations in the canonical (constant number of particles, volume, and temperature) ensemble were run [55]. Particles were introduced into a cubic box, allowed to interact pairwise, and subjected to minimum image convention to minimize interface effects. Each simulation was equilibrated through 100 000 cycles and sampled for ten runs of 1 000 000 cycles. One move was attempted for every particle during one cycle. Maximum displacement was adjusted to reach a 50% acceptance ratio in Metropolis sampling. Temperature, density, and number of particles were varied. Pressure was calculated via the virial route [56] and direct evaluation of the derivative of the Helmholtz free energy with respect to volume [57], as first proposed by Eppenga and Frenkel for hard-core particles [58] and later expanded to soft-core potentials by Harismiadis *et al.* [59]. When setting test volume change to $\Delta V = 0.003V$ for the free-energy route, its results were in agreement with the virial route (difference was less than statistical uncertainty).

Umbrella sampling calculations were performed to obtain Gibbs free energies as a function of varying density and structure at a given temperature and pressure, as follows. A biasing potential was introduced as

$$\Delta U = k_1(\rho - \rho^0)^2 + k_2\left(Q_6 - Q_6^0\right)^2, \quad (3)$$

where ρ is the density of the system and Q_6 the bond-orientational order parameter. Superscripted quantities (ρ^0 and Q_6^0) are the so-called controlled density and bond-orientational order parameter, respectively, that are imposed upon the system. Q_6 was chosen because its value was observed to change noticeably upon crystallization and to differ between the low-density and high-density liquid phases. It falls to zero in completely disordered systems and increases as the system gets more structured. Thus it allowed us to prevent crystallization and to investigate the system reordering upon liquid-liquid phase transition. Q_6 was calculated as defined by Steinhardt *et al.* [60]. First, we calculated the averaged spherical harmonics of each molecule i with its twelve nearest neighbors. We opted for twelve particles because the model does not account for preferential tetrahedral bonding and instead uses the isotropic potential:

$$q_{l,m}^i = \frac{1}{12}\sum_{j=1}^{12} Y_l^m(\theta_{ij},\phi_{ij}), \quad (4)$$

where Y_l^m is the spherical harmonic function of the angular coordinates of the vector between the centers of mass of the molecules i and j. We set $l = 6$ and first sum across the harmonics

$$Q_6^i = \sqrt{\frac{4\pi}{13}\sum_{m=-6}^{m=6}\left|q_{6,m}^i\right|^2} \quad (5)$$

and then across all particles

$$Q_6 = \frac{1}{N}\sum_{i=1}^{N} Q_6^i. \quad (6)$$

After each cycle, biasing potential with values $k_1 = k_2 = 500\,000$ is calculated and Metropolis sampling used to check whether to accept the cycle or not, yielding approximately 40% acceptance ratio. Chemical potential, μ, of a system is calculated with the Widom insertion method, where a ghost particle is inserted at random and its interaction, U, with every other particle is calculated. This is possible because the system is not so dense that it would hinder the applicability and accuracy of this method:

$$\mu = -k_B T \ln\left[\langle V\rangle_N^{-1}\langle V\exp\left(-\beta U\right)\rangle_N\right]. \quad (7)$$

It was noted that Q_6 is between 0.290 and 0.300 in the liquid phases and above 0.370 when crystallization begins to occur. Thus we can limit our investigation to the liquid range.

IV. RESULTS AND DISCUSSION

In Fig. 2 we display isotherms as obtained from simulations using 512 particles. Oscillatory parts of the isotherms are

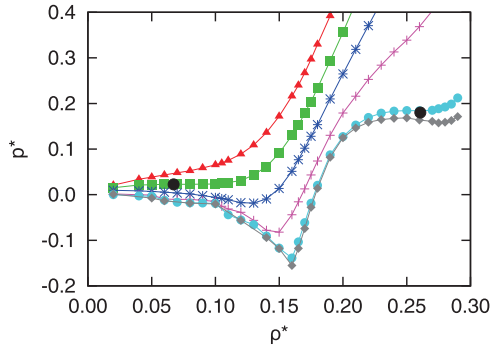

FIG. 2. (Color online) Isotherms (p^* vs ρ^*) for the model of methanol studied. Symbols (triangles $T^* = 1.30$, squares $T^* = 1.09$, stars $T^* = 0.9$, crosses $T^* = 0.7$, circles $T^* = 0.54$, and diamonds $T^* = 0.52$) are results of MC simulations; numerical error is smaller than the symbol size. Black full circles represent gas-liquid and liquid-liquid critical point. Connecting lines are a guide for the eye.

characteristic of a first-order phase transition. Critical point is by definition the saddle point on the critical isotherm. Below, a metastable area can be identified with the Maxwell construction [61]. We see two critical points, one corresponding to a typical liquid-gas phase transition and the other one to a liquid-liquid phase transition. Similar behavior was observed when using CSW to model water [34].

Critical phenomena are highly dependent on the size of the system, meaning that the location of the critical point is different for different system sizes. As the system approaches the critical point, the correlation length increases and for an infinite system goes to infinity as the critical temperature is approached. For finite-sized systems the correlation length reaches the system size before the critical point of an infinite system is reached. Consequently, the critical point is shifted compared to the infinite system. To compensate for this and to obtain the exact location of the critical points in bulk, we used a finite-size scaling test in the Ising universality class [62]. Simulations were run with 128, 256, 512, or 1024 particles near both critical points at several temperatures. Points on each isotherm were fitted with a fifth-order polynomial and then repeatedly differentiated to obtain the exact position of the saddle point in each system.

TABLE I. Critical points for model of water [34] and methanol within the thermodynamic limit.

Model	Critical point type	T^*	ρ^*	p^*
CSW water	Gas-liquid	1.13	0.082	0.024
	Liquid-liquid	0.58	0.246	0.106
CSW methanol	Gas-liquid	1.076	0.0753	0.0206
	Liquid-liquid	0.503	0.2662	0.1539

We plot the critical density and critical temperature as functions of rescaled variables in Fig. 3. L is the cubic box size, d is the dimensionality of the system ($d = 3$), υ is the critical exponent of the correlation length ($\upsilon = 0.629$), and θ is the universal correction to the scaling exponent ($\theta = 0.54$) [62]. See Table I for the exact location of the critical points in methanol and water, as predicted by extrapolation to the infinite size ($L \to \infty$).

The second critical point (LLCP) is of particular interest. Figure 4 shows that the methanol molecules structure differently in the low-density and high-density regimes. Pair

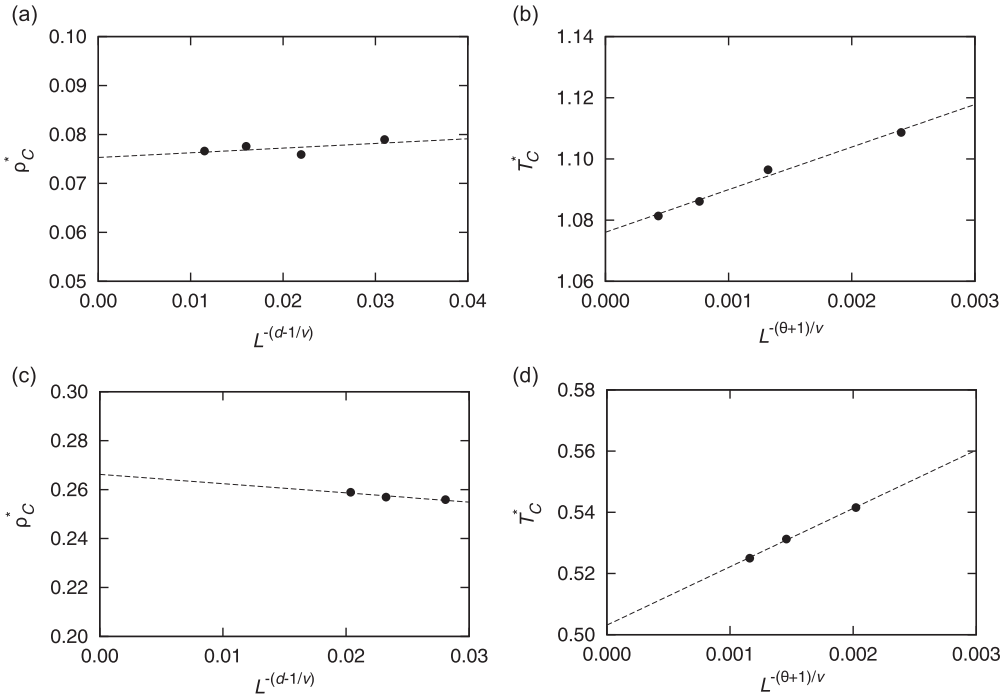

FIG. 3. Size dependence of the critical temperature and density for the modeled systems. (a) Critical density for gas-liquid transition. (b) Critical temperature for gas-liquid transition. (c) Critical density for liquid-liquid transition. (d) Critical temperature for liquid-liquid transition. Dashed lines represent best linear fits.

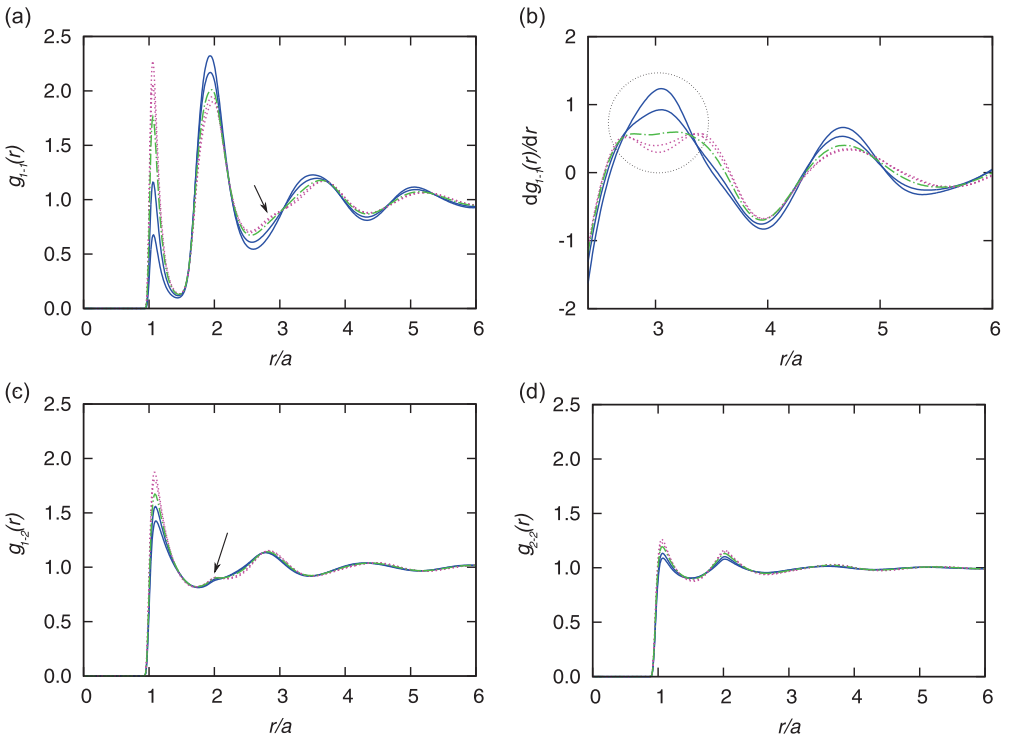

FIG. 4. (Color online) Site-site radial distribution functions between (a), (b) type 1 [(b) shows derivative], (c) type 1 and 2, and (d) type 2 particles show the difference in ordering of low-density and high-density liquid phases. In high-density phase (blue, solid line) ordering is higher than in low-density phase (purple, dotted line). Green (dot-dashed) line depicts ordering in the liquid-liquid critical point.

distribution function between hydroxyl groups [Fig. 4(a)] exhibits an inflection at $r/a = 3$ in the high-density regime, which is easy to spot if we plot its derivative [Fig. 4(b)]. Additional ordering of methanol in high-density regime is also visible in the pair distribution function between hydroxyl and methyl groups [Fig. 4(c)], where a small peak around $r/a = 2.3$ is observed in the high-density regime, but vanishes at lower densities. Methyl groups have no preferential orientation, as shown in their respective pair distribution function [Fig. 4(d)]. All site-site correlation functions show different long-range behavior in different phases.

To confirm the apparent difference in structure, we measure the root of mean-squared displacement (Δr) for particles as a Monte Carlo analog of the diffusion coefficient. In these simulation runs, dynamic adjustment of maximum displacement was turned off and was kept fixed at $dx_{\max} = 0.02L$ for all instances. Figure 5(a) shows Δr as a function of the number of steps. Densities from $\rho^* = 0.22$ up to $\rho^* = 0.28$ were investigated with a step of $\Delta\rho^* = 0.01$, all at temperature $T^* = 0.52$. These curves were fitted with polynomials $y = D^* x^{0.5}$ to obtain the provisional diffusion coefficient (D^*), depicted in Fig. 5(b). Results definitively prove a difference in the structure, as the trend in low-density and high-density regimes is different. Intersection is in the point of phase transition at this temperature. This is in agreement with theoretical treatment of the model with integral equations [63].

If the oscillations in the pressure-density plot stem from the liquid-liquid phase transition and not from the onset of crystallization, one would expect two basins of minimum chemical potential in the (ρ, Q_6) plane near the critical point.

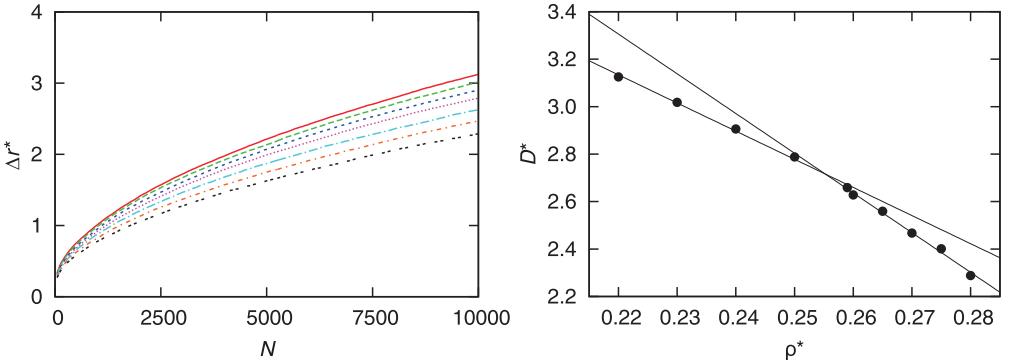

FIG. 5. (Color online) Average displacement per particle as a function of simulation cycles (left). Densities shown (from top to bottom line): $\rho^* = 0.22$, 0.23, 0.24, 0.25, 0.26, 0.27, and 0.28. (Right) Diffusion coefficient shown as a function of density of methanol.

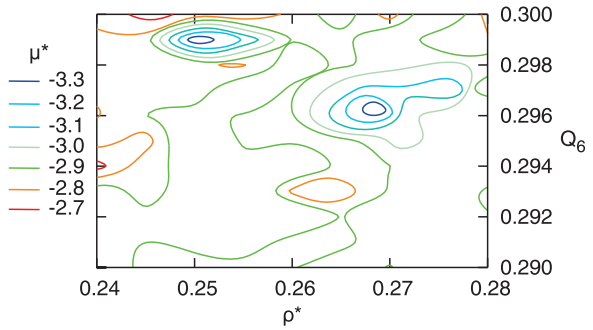

FIG. 6. (Color online) Free energy as a function of density, ρ^*, and bond-orientational order parameter, Q_6, in the vicinity of the liquid-liquid critical point. At $p^* = 0.200$ and $T^* = 0.52$, two basins of minimum free energy are visible.

Calculated chemical potential in the range $\rho^* = 0.24$–0.28 with a step 0.005 and $Q_6^* = 0.290$–0.300 with a step 0.001 at pressure $p^* = 0.200$ and temperature $T^* = 0.51$ is shown in Fig. 6. Note that, although higher than the critical temperature in bulk, this is below critical temperature for the investigated system, consisting of 512 particles. We can clearly see two minima that correspond to low-density and high-density liquid. Our aim was to use these data to prove the existence of liquid-liquid phase transition and not to ascertain the free energies with high accuracy as the latter would have a higher computational cost. Statistical uncertainty of free energies is around 5%, because the system is not too dense, which is good enough to claim the existence of two minima.

When run for extended periods of time, unbiased simulations in the vicinity of the second critical point resulted in imperfect crystallization of the system. Hydroxyl groups (CSW particles) assumed the positions of hexagonal close packing. Presumably due to weaker interactions, methyl groups (Lennard-Jones particles) did not exhibit any preferential orientations. Slightly above the temperature of this critical point, however, the crystal lattice melted. While the CSW water model exhibits the liquid-liquid critical point in the stable area, the CSW methanol model obviously shifts it to temperatures slightly below the freezing temperature. Similar behavior is believed to happen in real water, where the liquid-liquid critical point is postulated to occur in the deeply supercooled regime. Experimental data for methanol in the supercooled area is lacking.

Table II shows experimental data for critical points in water and methanol and the hydrogen bond strength and length. Data on liquid-liquid critical point in water have a large uncertainty because it occurs in the supercooled region that is impossible to evaluate directly. Hydrogen bond parameters are known more precisely, but there is still great variation among reported values in literature [64–69].

TABLE III. Predicted critical points of methanol from our model.

Critical point type	T (K)	ρ (kg m^{-3})	p (MPa)
Gas-liquid	513	240	12
Liquid-liquid	163	845	27

We use these data in conjunction with the model-predicted critical points to provide an estimation for the location of the tentative liquid-liquid critical point in real methanol. Taking into account slightly different hydrogen bond length and strength in methanol as compared to water and inherent differences between the models, we evaluate the position of methanol critical points as $T = T^{\mathrm{expt}}_{\mathrm{water}} \frac{T^*_{\mathrm{methanol}}}{T^*_{\mathrm{water}}} \frac{E_{\mathrm{methanol}}}{E_{\mathrm{water}}}$, $\rho = \rho^{\mathrm{expt}}_{\mathrm{water}} \frac{T^*_{\mathrm{methanol}}}{T^*_{\mathrm{water}}} \frac{a^3_{\mathrm{water}}}{a^3_{\mathrm{methanol}}}$, and $p = p^{\mathrm{expt}}_{\mathrm{water}} \frac{T^*_{\mathrm{methanol}}}{T^*_{\mathrm{water}}} \frac{E_{\mathrm{methanol}}}{E_{\mathrm{water}}} \frac{a^3_{\mathrm{water}}}{a^3_{\mathrm{methanol}}}$. Asterisked quantities are dimensionless simulation results, E is the experimentally determined hydrogen bond strength, and a is its length. Table III shows that this treatment gives an estimation for the liquid gas critical in methanol that is fairly close to experimental data. We then use it to predict the location of the liquid-liquid critical point in methanol around $T = 163$ K, $\rho = 845$ kg m^{-3}, and $p = 27$ MPa. However, some caution should be taken since those values are highly dependent on the input parameters (bond strength, length, and location of water LLCP). Upon changing those parameters, the location of methanol LLCP varies as well.

V. CONCLUSION

Reported results constitute considerable evidence for the existence of a liquid-liquid critical point in methanol, which has been observed experimentally here. We used a spherically symmetric coarse-grained methanol as its analogs have already been used to successfully model methanol nonidealities and water anomalies. The hydroxyl group was modeled with continuous shouldered well potential, while the methyl group is described with a Lennard-Jones–like potential. Simulation results reveal the existence of two critical points, one corresponding to gas-liquid phase transition and the other one to liquid-liquid phase transition. This findings are corroborated by free-energy estimation in the vicinity of the critical point, where two minima are observed. The structural difference between high- and low-density liquid phases is confirmed by the radial distribution functions and quasidiffusion coefficient. We demonstrate reordering in the high-density phase and slower diffusion.

TABLE II. Experimentally observed critical points in water and methanol and H-bond strength and length in water and methanol. Note that the estimates for hydrogen bond strength in methanol vary greatly in literature [64–69].

Substance	Critical point type	T (K)	ρ (kg m^{-3})	p (MPa)	H-bond strength (kJ mol^{-1})	H-bond length (Å)
Water	Gas-liquid [70]	647	322	22	21 [71]	2.8 [72]
	Liquid-liquid [13,73]	227	960	27.5		
Methanol	Gas-liquid [74]	513	272	8	17.5 [64]	3 [64]

In simulations below the temperature of liquid-liquid critical point, the system assumed a quasicrystal state after a prolonged number of simulation cycles, which was demonstrated with sharply peaked pair distribution functions and a decrease of the quasidiffusion coefficient for one order of magnitude. Umbrella sampling was used to avoid crystallization and study the basins of free energy in the vicinity of the critical point. This shows that the liquid-liquid phase transition occurs in the supercooled range.

Combining existing experimental data on water and methanol and results of our simulations, we have pinpointed an approximate region where the LLCP of methanol should reside. Similar to water, it appears to be located in the supercooled range of the phase diagram, making it rather challenging to study experimentally. These results give insights into the understanding of water and methanol behavior.

ACKNOWLEDGMENTS

This work was made possible by the support of the Slovenian Research Agency (Grant No. P1 0103-0201), NIH (Grant No. GM063592), and the Slovenian "Young Researcher" programme.

[1] D. Eisenberg and W. Kauzmann, *The Structure and Properties of Water*, 1st ed. (Oxford University Press, Oxford, 1969).
[2] F. Franks and D. S. Reid, *Water. A Comprehensive Treatise*, 1st ed. (Plenum Press, New York, 1973), Vol. 2.
[3] M. F. Chaplin, Biochem. Mol. Biol. Educ. **29**, 54 (2001).
[4] R. Sharma, S. N. Chakraborty, and C. Chakravarty, J. Chem. Phys. **125**, 204501 (2006).
[5] Y. D. Fomin, V. N. Ryzhov, and E. E. Tareyeva, Phys. Rev. E **74**, 041201 (2006).
[6] N. V. Gribova, Y. D. Fomin, D. Frenkel, and V. N. Ryzhov, Phys. Rev. E **79**, 051202 (2009).
[7] P. H. Poole, F. Sciortino, U. Essman, and H. E. Stanley, Nature (London) **360**, 324 (1992).
[8] J. W. Biddle, V. Holten, J. V. Sengers, and M. A. Anisimov, Phys. Rev. E **87**, 042302 (2013).
[9] L. Liu, S.-H. Chen, A. Faraone, C.-W. Yen, and C.-Y. Mou, Phys. Rev. Lett. **95**, 117802 (2005).
[10] H. E. Stanley, C. A. Angell, U. Essmann, M. Hemmati, P. H. Poole, and F. Sciortinoa, Physica A **205**, 122 (1994).
[11] D. A. Fuentevilla and M. A. Anisimov, Phys. Rev. Lett. **97**, 195702 (2006).
[12] D. T. Limmer and D. Chandler, J. Chem. Phys **135**, 134503 (2011).
[13] V. Holten, C. E. Bertrand, M. A. Anisimov, and J. V. Sengers, J. Chem. Phys. **136**, 094507 (2012).
[14] D. T. Holten, V. Limmer, V. Molinero, and M. A. Anisimov, J. Chem. Phys. **138**, 174501 (2013).
[15] A. Nilsson and L. G. M. Pettersson, Chem. Phys. **389**, 1 (2011).
[16] O. Mishima and H. E. Stanley, Nature (London) **396**, 329 (1998).
[17] K.-i. Murata and H. Tanaka, Nat. Mater. **11**, 436 (2012).
[18] A. K. Soper and M. A. Ricci, Phys. Rev. Lett. **84**, 2881 (2000).
[19] C. Un Kim, B. Barstow, M. W. Tate, and S. M. Gruner, Proc. Natl. Acad. Sci. USA **106**, 4596 (2009).
[20] K. Winkel, E. Mayer, and T. Loerting, J. Phys. Chem. B **115**, 14141 (2011).
[21] H. E. Stanley and J. Teixeira, J. Phys. Chem. **73**, 3404 (1980).
[22] S. Sastry, P. G. Debenedetti, F. Sciortino, and H. E. Stanley, Phys. Rev. E **53**, 6144 (1996).
[23] P. A. Netz, F. W. Starr, M. C. Barbosa, and H. E. Stanley, Physica A **314**, 470 (2002).
[24] A. B. de Oliveira, P. A. Netz, and M. C. Barbosa, Eur. Phys. J. B **64**, 481 (2008).
[25] M. A. A. Barbosa, E. Salcedo, and M. C. Barbosa, Phys. Rev. E **87**, 032303 (2013).
[26] R. L. Lundblad and F. Macdonald, *Handbook of Biochemistry and Molecular Biology*, 4th ed. (CRC Press, Boca Raton, FL, 2010).
[27] W. L. Jorgensen, J. Chandrasekhar, J. D. Madura, R. W. Impey, and M. L. Klein, J. Chem. Phys. **79**, 926 (1983).
[28] H. J. C. Berendsen, J. R. Grigera, and T. P. Straatsma, J. Phys. Chem. **91**, 6269 (1987).
[29] W. L. Jorgensen and J. D. Madura, Mol. Phys. **56**, 1381 (1985).
[30] M. W. Mahoney and W. J. Jorgensen, J. Chem. Phys. **112**, 8910 (2000).
[31] C. L. Dias, T. Ala-Nissila, M. Grant, and M. Karttunen, J. Chem. Phys. **131**, 054505 (2009).
[32] C. Dias, T. L. Hynninen, T. Ala-Nissila, A. S. Foster, and M. Karttunen, J. Chem. Phys. **134**, 065106 (2011).
[33] A. Bizjak, T. Urbic, V. Vlachy, and K. A. Dill, J. Chem. Phys. **131**, 194504 (2009).
[34] M. Huš and T. Urbic, J. Chem. Phys. **139**, 114504 (2013).
[35] S. V. Buldyrev, P. Kumar, P. G. Debenedetti, P. J. Rossky, and H. E. Stanley, Proc. Natl. Acad. Sci. USA **104**, 20177 (2007).
[36] E. A. Jagla, J. Chem. Phys. **111**, 8980 (1999).
[37] A. Chaimovich and M. S. Shell, Phys. Rev. E **88**, 052313 (2013).
[38] M. Huš and T. Urbic, Phys. Rev. E **90**, 022115 (2014).
[39] M. E. Johnson, T. Head-Gordon, and A. A. Louis, J. Chem. Phys. **126**, 144509 (2007).
[40] M. Huš and T. Urbic, J. Chem. Phys. **140**, 144904 (2014).
[41] J. R. Dowdle, S. V. Buldyrev, H. E. Stanley, P. G. Debenedeti, and P. J. Rossky, J. Chem. Phys. **138**, 064506 (2013).
[42] S. Garde and H. S. Ashbaugh, J. Chem. Phys. **115**, 977 (2001).
[43] S. Garde, G. Hummer, A. E. Garcia, M. E. Paulaitis, and L. R. Pratt, Phys. Rev. Lett. **77**, 4966 (1996).
[44] M. Maiti, S. Weiner, S. V. Buldyrev, H. E. Stanley, and S. Sastry, J. Chem. Phys. **136**, 044512 (2012).
[45] S. Sharma, S. K. Kumar, S. V. Buldyrev, P. G. Debenedetti, P. J. Rossky, and H. E. Stanley, Sci. Rep. **3**, 1841 (2013).
[46] F. Saija, S. Prestipino, and G. Malescio, Phys. Rev. E **80**, 031502 (2009).
[47] S. Prestipino, F. Saija, and G. Malescio, J. Chem. Phys. **133**, 144504 (2010).
[48] G. Malescio and F. Saija, J. Phys. Chem. B **115**, 14091 (2011).
[49] G. Franzese, J. Mol. Liq. **136**, 267 (2007).
[50] B. Hribar-Lee and K. A. Dill, Acta Chim. Slov. **53**, 257 (2006).
[51] H. Tanaka, J. Walsh, and K. E. Gubbins, Mol. Phys. **76**, 1221 (1992).

[52] E. J. W. Wensink, A. C. Hoffmann, P. J. van Maaren, and D. van der Spoel, J. Chem. Phys. **119**, 7308 (2003).
[53] D. González-Salgado and I. Nezbeda, Fluid Phase Equilib. **240**, 161 (2006).
[54] Z. Su, S. V. Buldyrev, P. G. Debenedeti, P. J. Rossky, and H. E. Stanley, J. Chem. Phys. **136**, 044511 (2012).
[55] M. P. Allen and D. J. Tildesley, *Computer Simulations of Liquids*, 1st ed. (Oxford University Press, Oxford, 1989).
[56] J.-P. Hansen and I. R. McDonald, *Theory of Simple Liquids*, 3rd ed. (Academic Press, London, 2006).
[57] E. de Miguel and G. Jackson, J. Chem. Phys. **125**, 164109 (2006).
[58] R. Eppenga and D. Frenkel, Mol. Phys. **52**, 1303 (1984).
[59] V. I. Harismiadis, J. Vorholz, and A. Z. Panagiotopoulos, J. Chem. Phys. **105**, 8469 (1996).
[60] P. J. Steinhardt, D. R. Nelson, and M. Ronchetti, Phys. Rev. B **28**, 784 (1983).
[61] J. C. Maxwell, Nature (London) **11**, 357 (1875).
[62] N. B. Wilding, J. Phys.: Condens. Matter **9**, 585 (1997).
[63] M. Huš, G. Munaò, and T. Urbic, J. Chem. Phys. **141**, 164505 (2014).
[64] C. Czeslik and J. Jonas, Chem. Phys. Lett. **302**, 633 (1999).
[65] H. G. M. Edwards and D. W. Farwell, J. Mol. Struct. **220**, 217 (1990).
[66] E. M. Schulman, D. W. Dwyer, and D. C. Doetschman, J. Phys. Chem. **94**, 7308 (1990).
[67] C. M. V. Taylor, S. Bai, C. L. Mayne, and D. M. Grant, J. Phys. Chem. B **101**, 5652 (1997).
[68] J. L. Fulton, G. G. Yee, and R. D. Smith, J. Am. Chem. Soc. **113**, 8327 (1991).
[69] M. M. Hoffmann and M. S. Conradi, J. Phys. Chem. B **102**, 263 (1998).
[70] Y. Marcus, *Supercritical Water*, 2nd ed. (Wiley, Hoboken, NJ, 2012).
[71] T. R. Dyke, J. Chem. Phys. **66**, 492 (1977).
[72] M. Huš and T. Urbic, J. Chem. Phys. **136**, 144305 (2012).
[73] C. E. Bertrand and M. A. Anisimov, J. Phys. Chem. B. **115**, 14099 (2011).
[74] R. G. Goodwin, J. Phys. Chem. Ref. Data **16**, 799 (1987).